

Small-signal amplification in bifurcating dynamical systems

Kurt Wiesenfeld* and Bruce McNamara

Department of Physics, University of California, Santa Cruz, California 95064

(Received 5 August 1985)

Near the onset of a dynamical instability, any time-periodic system can act to amplify small periodic perturbations. The details of this small-signal sensitivity depend solely on the type of bifurcation involved: Explicit expressions are derived for the power spectra in the vicinity of the simplest classes of codimension-1 bifurcations. Results obtained from analog simulations of a period-doubling system are in good agreement with the theory. We propose that the superconducting Josephson-junction parametric amplifier is an example of this amplification process.

I. INTRODUCTION

This paper concerns time-periodic dynamical systems near the onset of instabilities and their sensitivity to perturbations which are likewise periodic. We show that such dynamical systems can greatly amplify small-amplitude perturbations, provided the frequency of the perturbation is properly chosen. The "proper choice" of frequency range depends only on the type of bifurcation encountered. In this paper we consider several classes of bifurcation: saddle-node, transcritical, pitchfork, period-doubling, and Hopf. These are the simplest codimension-1 instabilities of periodic orbits. i.e., they are the bifurcations typically encountered as a single control parameter is varied. The results of this paper are based on very general considerations; consequently, they apply to any physical system governed by a set of ordinary differential equations, near the onset of a bifurcation.

The basic principles involved here have already appeared in a short paper.¹ There, we studied a particular system, namely the driven Duffing equation

$$\ddot{x} + \gamma \dot{x} + \lambda_0 x + \beta x^3 = A \cos(\omega t) + B + \delta \cos(\Omega t), \quad (1.1)$$

where the constants γ , λ_0 , β , A , and B were tuned so that the unperturbed oscillator ($\delta=0$) was close to the onset of a period doubling. When the small-amplitude modulation was turned on ($\delta \neq 0$) with frequency $\Omega \approx n\omega/2$, n an odd integer, the power spectrum of $x(t)$ showed a large component at Ω . An explicit expression for the power spectrum was derived for Eq. (1.1) in terms of the detuning frequency $\Delta = \Omega - n\omega/2$ and the bifurcation parameter ϵ when both Δ and ϵ were small: Analog simulations of Eq. (1) were also performed, and these supported the analytic results.¹

The purpose of the present work is to extend the results of Ref. 1 in four important ways. First, we begin with the more general evolution equation

$$\dot{\mathbf{x}} = \mathbf{F}(\mathbf{x}, t), \quad \mathbf{x} \in \mathbb{R}^N. \quad (1.2)$$

Second, the unperturbed system may depend explicitly on time, as in Eq. (1.1), or may not (the system is said to be nonautonomous or autonomous, respectively). Third, the perturbative modulation can enter either additively as in

Eq. (1.1), or "parametrically," such as

$$\ddot{x} + \gamma \dot{x} + [\lambda_0 + \delta \cos(\Omega t)]x + \beta x^3 = A \cos(\omega t) + B. \quad (1.3)$$

Finally, the instability in question need not be a period-doubling bifurcation. We are able to handle most of these generalizations within a single notational formalism, the only exception being the difference between autonomous and nonautonomous systems. Consequently, the derivations for autonomous systems are covered separately in Sec. V, though the differences with the corresponding nonautonomous results are relatively mild.

The idea that a system poised near the onset of a dynamical instability might amplify coherent (i.e., non-random) signals was spawned from previous work concerning the effect of noisy perturbations on the power spectra of periodic systems.²⁻⁹ The addition of a flat-spectrum input (white noise) gives rise to new broadband peaks not present in the noise-free system.^{2,3} In each case these noisy precursor peaks are centered at the new frequencies that appear only after the bifurcation of the deterministic system. The theory of noise precursors has been checked quantitatively by measurements on voltage-driven p - n junctions for period doubling and Hopf cases.³ Noisy precursors have also been seen in experiments on semiconductor lasers⁴ and in analog circuits governed by Eq. (1.1).⁶

One question that is bound to arise is whether the small-signal sensitivity described in this paper has a practical use. One place where these ideas may find practical application is in the study of superconducting Josephson-junction parametric amplifiers ("paramps").¹⁰⁻¹⁹ These devices operate in an interesting frequency range (~ 35 GHz) and have achieved good gain in laboratory experiments,¹⁰⁻¹³ although undesirable noise characteristics¹⁴⁻¹⁹ thus far have prevented them from being technologically useful. We propose that the basic amplification mechanism underlying the operation of these paramps is just the dynamical explanation developed here, both for three-photon paramps¹ and for four-photon paramps. We enter a fuller discussion of this topic in Sec. IV B.

An issue of a more general nature is discussed in Sec. IV C, which may also be important for potential applications of this amplification mechanism. The theory finds

that large amplification factors are achieved when both the bifurcation parameter ϵ and the detuning frequency Δ are small. Consequently, significant amplification might be achieved in only narrow frequency windows. An interesting phenomenon can occur, however, that alleviates this difficulty, allowing for a wide and continuous tuning range for these high-gain windows. This phenomenon—the so-called virtual Hopf sequence^{6,7}—is quite common in low-dimensional systems,⁷ such as the Lorenz equations and the driven damped pendulum (which in turn describes the Josephson paramp dynamics mentioned above).

The contents of this paper are organized as follows. In Sec. II the basic problem is laid out along with the formal mathematical framework, and a general expression is derived for the system's response to the perturbation. In Sec. III expressions are derived for the power spectrum near the onset of saddle-node, transcritical, pitchfork, period-doubling, and Hopf bifurcations, when the unperturbed system is nonautonomous. Section IV discusses three specific aspects of these general results: (i) The results of analog simulations of the driven Duffing oscillator are presented, and compared with the period-doubling predictions; (ii) the connection with Josephson paramps is made, for both the three- and four-photon operating modes; (iii) the virtual Hopf phenomenon is described and is shown to provide certain advantages for tuning and stability in small-signal amplification. In Sec. V we return to the situation where the unperturbed system is autonomous and compare the expected power spectra on a case-by-case basis with the corresponding results of Sec. III. Finally, a brief summary of the limitations and conclusions of the theory is provided in Sec. VI.

II. PERTURBATIVE APPROACH

Our aim is to study the effect of a coherent (i.e., non-random) perturbation on a system near the onset of a dynamical instability. Before developing the general formalism, we consider a specific example.

The damped driven pendulum obeys

$$\ddot{\theta} + \gamma \dot{\theta} + \omega_0^2 \sin\theta = A \cos(\omega t) \quad (2.1)$$

and can undergo a sequence of bifurcations as A is increased from zero.^{15,20,21} For small driving amplitude A , the steady-state response $\theta(t)$ is a symmetric, $(2\pi/\omega)$ -periodic oscillation. [The "symmetry" of $\theta(t) = -\theta(t + \pi/\omega)$. The experimental signature of such an orbit is that its power spectrum contains odd harmonics only.] As A is increased, the system first undergoes a symmetry-breaking, or *pitchfork*, bifurcation. Then, steadily increasing A can result in a sequence of period-doubling bifurcations, leading to chaos.^{15,20,21}

Suppose that A is adjusted so that the system is just before the onset of the first period doubling. Then we will demonstrate that a small, coherent perturbation of the system will be amplified greatly when the frequency of the perturbation is close to $\omega/2$.

Generally speaking, there are two ways that a coherent signal can be coupled into Eq. (2.1). The small signal may enter *additively*, so that Eq. (2.1) becomes

$$\ddot{\theta} + \gamma \dot{\theta} + \omega_0^2 \sin\theta = A \cos(\omega t) + \delta \cos(\Omega t + \phi) . \quad (2.2)$$

Alternatively, one of the *parameters* may be modulated about its mean value, for example,

$$\ddot{\theta} + \gamma \dot{\theta} + [\omega_0^2 + \delta \cos(\Omega t + \phi)] \sin\theta = A \cos(\omega t) . \quad (2.3)$$

We can consider both additive and parametric modulation at the same time by the following device. Think of Eq. (2.1) as having an additional, constant term on the right-hand side. Then Eq. (2.2) represents a *parametric* modulation of that constant term, for the special case where its mean value is zero.

The general development begins with a dynamical system governed by the set of first-order nonlinear differential equations

$$\dot{\mathbf{x}} = \mathbf{F}(\mathbf{x}; \lambda), \quad \mathbf{x} \in R^N . \quad (2.4)$$

Here, \mathbf{F} may or may not depend explicitly on time, and \mathbf{F} depends on (at least) one parameter λ , which we take to be modulated about its mean value λ_0 :

$$\lambda = \lambda_0 + \delta \cos(\Omega t) . \quad (2.5)$$

The dependence of \mathbf{F} on any other parameters is suppressed for notational convenience.

We next suppose that the unperturbed ($\delta=0$) system has a stable periodic solution \mathbf{x}_0 :

$$\mathbf{x}_0(t + T) = \mathbf{x}_0(t) . \quad (2.6)$$

The effect of a weak perturbation ($\delta \neq 0$) is to make $\mathbf{x}(t)$ deviate from $\mathbf{x}_0(t)$. Writing this small deviation as $\boldsymbol{\eta} = \mathbf{x} - \mathbf{x}_0$, Eq. (2.4) becomes

$$\dot{\mathbf{x}}_0 + \dot{\boldsymbol{\eta}} = \mathbf{F}(\mathbf{x}_0 + \boldsymbol{\eta}; \lambda_0 + \delta \cos(\Omega t)) . \quad (2.7)$$

Expanding \mathbf{F} to first order in $\boldsymbol{\eta}$ and δ , and using the fact that \mathbf{x}_0 is a solution of Eq. (2.4) when $\delta=0$, leads to an evolution for $\boldsymbol{\eta}$:

$$\dot{\boldsymbol{\eta}} = D\mathbf{F}(\mathbf{x}_0; \lambda_0) \boldsymbol{\eta} + \delta \cos(\Omega t) \boldsymbol{\Lambda} , \quad (2.8)$$

where $D\mathbf{F}$ is the matrix of periodic functions

$$(D\mathbf{F})_{ij} = \frac{\partial F_i}{\partial x_j} \quad (2.9)$$

and $\boldsymbol{\Lambda}$ is the vector of periodic functions

$$\Lambda_i = \left[\frac{\partial F_i}{\partial \lambda} \right]_{\mathbf{x}=\mathbf{x}_0} . \quad (2.10)$$

For example, for the parametrically modulated system (2.3), we have $\lambda_0 = \omega_0^2$, and

$$\mathbf{x} = \begin{bmatrix} \theta \\ \dot{\theta} \end{bmatrix}, \quad D\mathbf{F} = \begin{bmatrix} 0 & 1 \\ -\omega_0^2 \cos\theta_0 & -\gamma \end{bmatrix},$$

$$\boldsymbol{\Lambda} = \begin{bmatrix} 0 \\ -\sin\theta_0 \end{bmatrix} .$$

In writing Eq. (2.8), terms of quadratic (and higher) degree in $\boldsymbol{\eta}$ have been ignored, leaving a linear inhomogeneous equation with periodic coefficients. Such equations can be solved via the standard methods of Floquet theory.²² We begin by recalling a few basic results needed to construct the solution to Eq. (2.8).

First, there exist special solutions ϕ_k of the homogeneous equation associated with Eq. (2.8), such that

$$\phi_k(t) = e^{\rho_k t} \mathbf{P}_k(t), \quad (2.11)$$

where \mathbf{P}_k is a periodic function with the same period as the matrix $D\mathbf{F}(\mathbf{x}_0; \lambda)$. For convenience, we assume that time is scaled so that this period is equal to 2π , so that

$$\mathbf{P}_k(t + 2\pi) = \mathbf{P}_k(t). \quad (2.12)$$

The constant ρ_k appearing in Eq. (2.11) is, in general, a complex quantity and is called a *Floquet exponent*. From Eq. (2.11) it is seen that ρ_k is arbitrary up to integer multiples of i . We remove this ambiguity by picking the branch

$$-\frac{1}{2}i < \text{Im}\rho_k \leq \frac{1}{2}i. \quad (2.13)$$

As will be shown, the Floquet exponents determine the main features of the observed power spectrum—all of the basic results can be neatly summarized in terms of the ρ_k .

Physically, the ϕ_k represent responses of the unmodulated ($\delta=0$) system to a single impulse perturbation. If the basic oscillation \mathbf{x}_0 is stable, these must not grow with time, so that

$$\text{Re}\rho_k \leq 0 \quad (2.14)$$

for all k . As the parameters of the system are tuned, the ρ_k vary. An instability is signaled when one or more of the ρ_k cross the imaginary axis into the right half-plane.

Typically, there will be N distinct Floquet exponents for the system (2.8); consequently there will be N linearly independent solutions ϕ_k . The importance of these solutions is that they may be used to construct a *fundamental matrix* $\Phi(t)$,

$$\Phi(t) = (\phi_1, \phi_2, \dots, \phi_N), \quad (2.15)$$

so that the j th column of Φ is ϕ_j . In terms of the matrix Φ , the solution of Eq. (2.8) may be written

$$\eta(t) = \Phi(t) \int_0^t \Phi^{-1}(t') [\delta \cos(\Omega t') \Lambda(t')] dt'. \quad (2.16)$$

In writing this, we have taken initial conditions $\eta(0)=0$ for convenience—the results of this paper are insensitive to the precise choice of $\eta(0)$.

The inverse matrix Φ^{-1} consists of row vectors

$$\Phi^{-1}(t') = \begin{bmatrix} e^{-\rho_1 t'} \mathbf{q}_1(t') \\ \vdots \\ e^{-\rho_N t'} \mathbf{q}_N(t') \end{bmatrix}, \quad (2.17)$$

where the \mathbf{q}_k , like the \mathbf{P}_k , are 2π -periodic functions of time. It is a simple matter to show that

$$\mathbf{P}_k \cdot \mathbf{q}_l = \delta_{kl}, \quad (2.18)$$

where δ_{kl} is the Kronecker delta, a fact which follows immediately because Φ and Φ^{-1} are inverse matrices.

In component notation, Eq. (2.16) becomes

$$\eta_m = \delta \sum_{k,l} \Phi_{mk}(t) \int_0^t (\Phi^{-1})_{kl}(t') \Lambda_l(t') \cos(\Omega t') dt' \quad (2.19)$$

with

$$\Phi_{mk} = e^{\rho_k t} P_{km} \quad (2.20)$$

and

$$(\Phi^{-1})_{kl} = e^{-\rho_k t} q_{kl}, \quad (2.21)$$

where P_{km} is the m th component of \mathbf{P}_k , and q_{kl} is the l th component of \mathbf{q}_k . Combining Eqs. (2.19)–(2.21) yields

$$\eta_m(t) = \delta \sum_{k,l} P_{km}(t) \int_0^t e^{\rho_k(t-t')} q_{kl}(t') \Lambda_l(t') \cos(\Omega t') dt' \quad (2.22)$$

which is the major result of this section. Note that this represents an exact solution to the linearized Eq. (2.8).

We now make an important observation: In the vicinity of a dynamical instability, $\eta_m(t)$ reduces to a particularly simple form. This is because the sum over k is dominated by only a small number of terms, corresponding to the number of near-critical exponent(s) ρ_k . In Sec. III we compute $\eta_m(t)$ and the corresponding power spectrum $S_m(\omega)$ for systems near the onset of the simplest classes of codimension-1 bifurcations of a periodic orbit. We will find that only the *type* of bifurcation encountered is important in determining the response of the system at the modulation frequency Ω . Moreover, there is a set of resonance frequencies determined solely by the bifurcation encountered, this resonance becoming stronger and sharper as the instability is approached.

III. POWER SPECTRA—DRIVEN SYSTEMS

In this section we compute the power spectra expected in the vicinity of various codimension-1 bifurcations. Generically, the basic oscillation \mathbf{x}_0 will go unstable in one of three ways as a single parameter is varied.

(i) A single real exponent ρ_1 crosses the imaginary axis. Usually, three subcases are distinguished depending on constraints and/or symmetries obeyed by the system. In what follows, only symmetry properties are important, so we will distinguish two cases: unsymmetric (saddle-node and transcritical bifurcations) and symmetric (pitchfork bifurcation).

(ii) A single exponent ρ_1 crosses the imaginary axis along the line $\text{Im}\rho = \frac{1}{2}$. From Eq. (2.11), one sees that this corresponds to a period-doubling instability, since—precisely at the bifurcation point—the function ϕ_1 simply changes sign after each 2π time interval.

(iii) A complex-conjugate pair $\rho_1, \rho_2 = \rho_1^*$ cross the imaginary axis with imaginary part different from zero or one-half. This corresponds to a Hopf bifurcation: In most cases the resulting orbits are confined to an invariant torus.²³

Before proceeding to the case-by-case derivation of the power spectrum, an important distinction between autonomous and nonautonomous systems must be made. In an autonomous system, time does not explicitly enter the differential equations, and there is *always* one Floquet exponent—call it ρ_N —equal to zero. Geometrically, this corresponds to the fact that, in phase space, the periodic orbit is neutrally stable to perturbations along the limit cycle. In the calculations that follow, the dominant con-

tribution to the power spectrum near an instability comes from exponents closest to the imaginary axis—consequently, both the near-critical exponent(s) and the zero exponent ρ_N contribute in the autonomous case. For driven systems, however, there is no such constraint on ρ_N . As we shall see, the prime effect of the zero exponent is to re-normalize the strength of the δ functions in the power spectrum due to the basic oscillation \mathbf{x}_0 ; moreover, since the exponent ρ_N is not free to move as the control parameters are varied, this extra “autonomous contribution” changes only mildly as the bifurcation is approached. In contrast, the contribution of the near-critical exponent(s) is quite sensitive to the value of the bifurcation parameter.

For the sake of clarity, we derive the expected power spectra for nonautonomous systems in this section, returning to the derivations relevant to autonomous systems in Sec. V.

A. Case one: Saddle-node and transcritical bifurcations

In this case, a single real exponent lies close to the origin

$$\rho_1 = -\epsilon, \quad (3.1)$$

where ϵ is a small positive number, and is the natural bifurcation parameter, since it is zero at the bifurcation point. With the other exponents relatively far from the imaginary axis, the sum in Eq. (2.22) is dominated by the $k = 1$ term:

$$\eta_m(t) = \delta P_{1m}(t) \int_0^t e^{\epsilon(t'-t)} \left[\sum_l q_{1l}(t') \Lambda_l(t') \right] \cos(\Omega t') dt'. \quad (3.2)$$

The function q_{1l} is 2π periodic and Λ_l is either constant (for additive modulations) or 2π periodic (for parametric modulations), so we may introduce the Fourier sum

$$\sum_l q_{1l}(t') \Lambda_l(t') = \sum_n \alpha_n e^{int'}, \quad \alpha_{-n} = \alpha_n^*, \quad (3.3)$$

this last condition following since the quantity is real. Equation (3.2) may be rewritten

$$\eta_m(t) = \frac{1}{2} \delta P_{1m}(t) \sum_n \alpha_n \int_0^t e^{\epsilon(t'-t)} e^{int'} (e^{-i\Omega t'} + e^{i\Omega t'}) dt'. \quad (3.4)$$

This integral is easily evaluated, yielding

$$\eta_m = \frac{1}{2} \delta P_{1m} \sum_n \left[\alpha_n \frac{e^{i(n-\Omega)t}}{\epsilon + i(n-\Omega)} + \text{c.c.} \right], \quad (3.5)$$

where c.c. means complex conjugate, and we have taken $\epsilon t \gg 1$. This last inequality simply means that the time series considered is of much longer duration than the longest dynamical time scale, which is required for determining a sensible power spectrum.

From Eq. (3.5), one sees that the response η_m will be large provided that the modulation frequency Ω is very close to an integer. Thus, we put

$$\Omega = k + \Delta, \quad |\Delta| \ll 1 \quad (3.6)$$

where k is an integer. Then the $n = k$ ($n = -k$) term dominates the sum over the first (second) part in large parentheses in Eq. (3.5), with the result

$$\eta_m = \frac{1}{2} \delta P_{1m} \left[\alpha_k \frac{e^{-i\Delta t}}{\epsilon - i\Delta} + \text{c.c.} \right]. \quad (3.7)$$

Finally, introducing the Fourier series

$$P_{1m}(t) = \sum_j \beta_j e^{ijt}, \quad \beta_{-j} = \beta_j^* \quad (3.8)$$

the power spectrum $S_m(\omega)$ corresponding to Eq. (3.7) is given by

$$S_m(\omega) = \frac{1}{4} \delta^2 \sum_j \frac{|\beta_j \alpha_k|^2}{\epsilon^2 + \Delta^2} [\delta(\omega - j - \Delta) + \delta(\omega - j + \Delta)]. \quad (3.9)$$

Note that the denominator is the sum of two small quantities, ϵ^2 and Δ^2 . Consequently, the small input modulation at frequency $k + \Delta$ gives rise to a relatively large response at frequencies $j \pm \Delta$ for all integers j . The situation is illustrated in Fig. 1, where the spectral lines at $\omega = 0, 1, 2, \dots$ due to the basic oscillation $\mathbf{x}_0(t)$ have also been included. For fixed bifurcation parameter ϵ , the frequency response S_m is a Lorentzian function of Δ , with half-width ϵ and height proportional to ϵ^{-2} .

B. Case two: Pitchfork (symmetry-breaking) bifurcation

In one sense, this is a special case since it requires that the dynamical system under study has a symmetry. On the other hand, symmetries are fairly common in physical systems, and in such systems symmetry-breaking bifurcations play an important role in the observed dynamics.^{24,25}

Here we have a specific symmetry in mind, in which the vector field $\mathbf{F}(\mathbf{x}, t)$ [see Eq. (2.4)] satisfies²⁶

$$\mathbf{F}(\mathbf{x}, t) = -\mathbf{F}(-\mathbf{x}, t + T/2), \quad (3.10)$$

where T is the period of \mathbf{F} , if it is explicitly time dependent. This is a common symmetry—for example, the

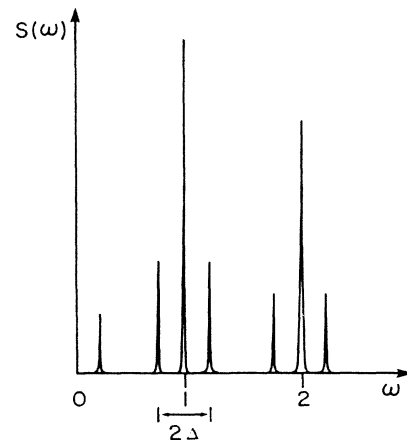


FIG. 1. Predicted power spectrum $S(\omega)$ for a periodically perturbed system near the onset of a saddle-node or transcritical bifurcation, as given by Eq. (3.9).

driven Duffing equation (1.1) with $B=\delta=0$ possesses property (3.10), as does the driven pendulum equation (2.1).

When property (3.10) holds, the (periodic) solution \mathbf{x}_0 may or may not share this symmetry. If it does, then

$$\mathbf{x}_0(t+T/2) = -\mathbf{x}_0(t). \quad (3.11)$$

Typically, a symmetric solution will lose stability by giving rise to a pair of asymmetric solutions²⁶—such a symmetry-breaking bifurcation is called a pitchfork bifurcation in the theory of iterated maps.²³ Near the onset of the instability, a single real exponent lies near the origin,

$$\rho_1 = -\epsilon, \quad (3.12)$$

while the other exponents have relatively large (negative) real parts, so that the sum in Eq. (2.22) is again dominated by the $k=1$ term:

$$\eta_m = \delta P_{1m}(t) \int_0^t e^{\epsilon(t'-t)} \sum_l q_{1l}(t') \Lambda_l(t') \cos(\Omega t') dt'. \quad (3.13)$$

We have assumed that time is scaled so that the matrix $D\mathbf{F}(\mathbf{x}_0)$ [see Eq. (2.9)] and thus $q_{1l}(t')$ are 2π periodic. Owing to the symmetry (3.11), the basic oscillation \mathbf{x}_0 is 4π periodic. It follows that Λ_l is either a constant (for an additive modulation) or a 4π -periodic symmetric function (for a parametric modulation). In the former instance, the product $q_{1l}\Lambda_l$ is 2π periodic,

$$\sum_l q_{1l}\Lambda_l = \sum_n \alpha_n e^{in t'}, \quad (3.14)$$

while a parametric modulation entails this product being 4π periodic and symmetric,

$$\sum_l q_{1l}\Lambda_l = \sum_{n \text{ odd}} \tilde{\alpha}_n e^{in t'/2}. \quad (3.15)$$

As before, the integral appearing in Eq. (3.13) is readily evaluated, with the results

$$\eta_m = \frac{1}{2} \delta P_{1m} \sum_n \left[\alpha_n \frac{e^{i(n-\Omega)t}}{\epsilon + i(n-\Omega)} + \text{c.c.} \right] \quad (3.16)$$

for an additive modulation, and

$$\eta_m = \frac{1}{2} \delta P_{1m} \sum_{n \text{ odd}} \left[\tilde{\alpha}_n \frac{e^{i(n/2-\Omega)t}}{\epsilon + i(n/2-\Omega)} + \text{c.c.} \right] \quad (3.17)$$

for a parametric modulation. An important difference thus appears between these two subcases: The system response η_m will be large for additive modulations near integer frequencies k ,

$$\Omega = k + \Delta, \quad (3.18a)$$

with the results

$$\eta_m = \frac{1}{2} \delta P_{1m} \left[\frac{\alpha_k e^{-i\Delta t}}{\epsilon - i\Delta} + \text{c.c.} \right], \quad (3.19a)$$

$$S_m(\omega) = \frac{1}{4} \delta^2 \sum_j \frac{|\beta_j \alpha_k|^2}{\epsilon^2 + \Delta^2} [\delta(\omega - j - \Delta) + \delta(\omega - j + \Delta)], \quad (3.20a)$$

whereas a large response requires parametric modulations to be near half-integer frequencies

$$\Omega = \frac{1}{2}k + \Delta, \quad k \text{ odd} \quad (3.18b)$$

so that

$$\eta_m = \frac{1}{2} \delta P_{1m} \left[\frac{\tilde{\alpha}_k e^{-i\Delta t}}{\epsilon - i\Delta} + \text{c.c.} \right], \quad (3.19b)$$

and

$$S_m(\omega) = \frac{1}{4} \delta^2 \sum_j \frac{|\beta_j \tilde{\alpha}_k|^2}{\epsilon^2 + \Delta^2} [\delta(\omega - j - \Delta) + \delta(\omega - j + \Delta)]. \quad (3.20b)$$

In writing Eqs. (3.20a) and (3.20b) we have used the Fourier series (3.8) for $P_{1m}(t)$. The power spectra for the two subcases are essentially identical. The observed spectrum, including the δ function at $\delta = \frac{1}{2}, \frac{3}{2}, \frac{5}{2}, \dots$, due to the basic symmetric oscillation \mathbf{x}_0 is illustrated in Fig. 2.

At first glance, it seems strange that the two types of modulation, which require input oscillations at different frequencies, lead to qualitatively identical power spectra. The mystery disappears, however, when one recalls that the actual input perturbation is given by the *product* $\Lambda_l \cos \Omega t$. Near a pitchfork bifurcation, the system “resonates” with input signals near integer frequencies for *both* subcases. Thus, if Λ_l is constant (additive modulation), one requires $\Omega \approx \text{integer}$, while if Λ_l contains half-integer frequencies (parametric modulation) one requires $\Omega \approx \text{half-integer}$ as well.

C. Case three: Period-doubling bifurcation (Ref. 1)

Near the onset of a period-doubling bifurcation, a single exponent lies near the imaginary axis, with

$$\rho_1 = -\epsilon + i/2. \quad (3.21)$$

Retaining only the $k=1$ term in Eq. (2.22) yields

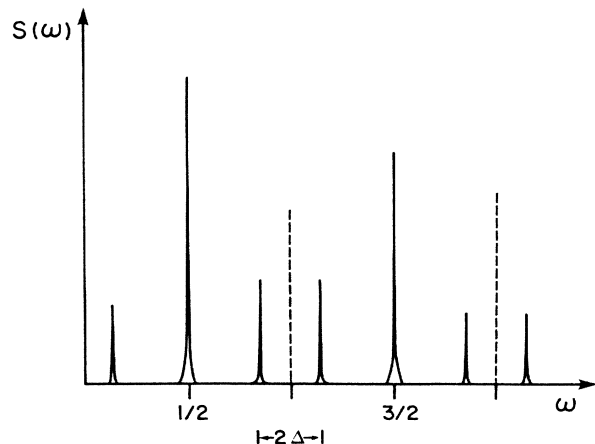


FIG. 2. Predicted power spectrum $S(\omega)$ for a periodically perturbed system near the onset of a pitchfork bifurcation, as given by Eq. (3.20).

$$\eta_m = \delta P_{1m} e^{it/2} \int_0^t e^{\epsilon(t'-t)} e^{-it'/2} \times \sum_l q_{1l}(t') \Lambda_l(t') \cos(\Omega t') dt' . \quad (3.22)$$

The product $q_{1l}\Lambda_l$ is 2π periodic, and $e^{-it'/2}$ merely changes sign after 2π , so we may introduce the Fourier series

$$e^{-it'/2} \sum_l q_{1l}(t') \Lambda_l(t') = \sum_{n \text{ odd}} \alpha_n e^{int'/2} . \quad (3.23)$$

Upon evaluating the integral in Eq. (3.22), we have

$$\eta_m = \frac{1}{2} \delta P_{1m} e^{it/2} \sum_{n \text{ odd}} \left[\alpha_n \frac{e^{i(n/2-\Omega)t}}{\epsilon + i(n/2-\Omega)} + \text{c.c.} \right] . \quad (3.24)$$

This will be large whenever

$$\Omega = k/2 + \Delta, \quad k \text{ odd} . \quad (3.25)$$

The dominant contribution to Eq. (3.24) becomes

$$\eta_m = \frac{1}{2} \delta P_{1m} e^{it/2} \left[\frac{\alpha_k e^{-i\Delta t}}{\epsilon - i\Delta} + \text{c.c.} \right] . \quad (3.26)$$

Since P_{1m} is 2π periodic, we may put

$$P_{1m}(t) e^{it/2} = \sum_{j \text{ odd}} \beta_j e^{ijt/2} \quad (3.27)$$

which is a 4π -periodic, symmetric function. Combining Eqs. (3.26) and (3.27) leads to the power spectrum

$$S_m(\omega) = \frac{1}{4} \delta^2 \sum_{j \text{ odd}} \frac{|\beta_j \alpha_k|^2}{\epsilon^2 + \Delta^2} [\delta(\omega - \frac{1}{2}j - \Delta) + \delta(\omega - \frac{1}{2}j + \Delta)] . \quad (3.28)$$

The situation is illustrated in Fig. 3. Analog simulations for the driven Duffing oscillator are presented in Sec. IV to test Eq. (3.28).

D. Case four: Hopf bifurcation

This final case entails a complex-conjugate pair of exponents ρ_1, ρ_2 crossing into the right half-plane. Just before the instability, we have

$$\rho_1 = -\epsilon + ib, \quad (3.29)$$

$$\rho_2 = \rho_1^*, \quad 0 < b < \frac{1}{2} .$$

Now only the two terms $k=1$ and 2 are retained in the summation appearing in Eq. (2.22):

$$\eta_m = \delta P_{1m} e^{ibt} \int_0^t e^{\epsilon(t'-t)} e^{-ibt'} \times \sum_l q_{1l}(t') \Lambda_l(t') \cos(\Omega t') dt' + \text{c.c.} , \quad (3.30)$$

where we have used the fact that, since ρ_1 and ρ_2 form a

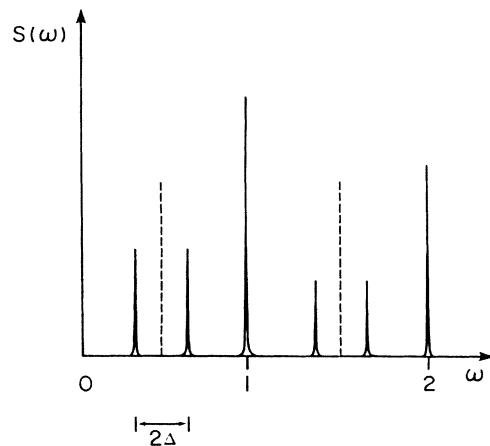


FIG. 3. Predicted power spectrum $S(\omega)$ for a periodically perturbed system near the onset of a period-doubling bifurcation, as given by Eq. (3.28).

complex-conjugate pair, $P_{1m} = P_{2m}^*$ and $q_{1l} = q_{2l}^*$. Introducing the Fourier expansion as before,

$$\sum_l q_{1l}(t') \Lambda_l(t') = \sum_{n \text{ odd}} \alpha_n e^{int'} , \quad (3.31)$$

the integral appearing in Eq. (3.30) reduces to

$$\frac{1}{2} \sum_n \alpha_n \left[\frac{e^{i(n-b-\Omega)t}}{\epsilon + i(n-b-\Omega)} + \frac{e^{i(n-b+\Omega)t}}{\epsilon + i(n-b+\Omega)} \right] . \quad (3.32)$$

(Note that $\alpha_{-n} \neq \alpha_n^*$ here since the function q_{1l} is complex.)

To get a large response η_m , let

$$\Omega = k + b + \Delta, \quad (3.33)$$

where k is an integer. Then the dominant contribution to (3.32) is

$$\frac{1}{2} \frac{\alpha_{-k} e^{i\Delta t}}{\epsilon + i\Delta} + \frac{1}{2} \frac{\alpha_k e^{-i\Delta t}}{\epsilon - i\Delta} . \quad (3.34)$$

Substitution of this into Eq. (3.30) yields

$$\eta_m = \frac{1}{2} \delta \sum_j \beta_j \left[\frac{\alpha_{-k}}{\epsilon + i\Delta} e^{i(j+b+\Delta)t} + \frac{\alpha_k}{\epsilon - i\Delta} e^{i(j+b-\Delta)t} \right] + \text{c.c.} , \quad (3.35)$$

where the Fourier expansion

$$P_{1m}(t) = \sum_j \beta_j e^{ijt} \quad (3.36)$$

has been introduced. Equation (3.35) leads to the power spectrum

$$\begin{aligned}
S(\omega) = & \frac{1}{4} \delta^2 \sum_j \frac{|\beta_j \alpha_{-k}|^2}{\epsilon^2 + \Delta^2} [\delta(\omega - j - b - \Delta) \\
& + \delta(\omega - j + b + \Delta)] \\
& + \frac{1}{4} \delta^2 \sum_j \frac{|\beta_j \alpha_k|^2}{\epsilon^2 + \Delta^2} [\delta(\omega - j - b + \Delta) \\
& + \delta(\omega - j + b - \Delta)] .
\end{aligned} \tag{3.37}$$

The situation is illustrated in Fig. 4 — a modulation introduced at the single frequency Ω gives rise to pairs of lines symmetrically located about half-integer frequencies. The occurrence in the present case of four lines between successive harmonics of the basic oscillation x_0 , rather than only two for the previous three cases, may be traced directly to the fact that there is a pair of near-critical exponents for the Hopf bifurcation.

Figure 5 summarizes the results of this section, showing the response of the system in terms of the near-critical exponent ρ_1 and the detuning frequency Δ . The dashed line represents the envelope of the new signal-induced line: The height and width of this envelope scales with $\text{Re}\rho_1$, while the center depends on $\text{Im}\rho_1$.

In general, the imaginary part b of the near-critical Floquet exponents may change as the parameters of the system are varied. As will be shown in Sec. IV, this feature is potentially important for exploiting the resonant mechanism discussed in this paper as a practical method for amplifying small signals.

IV. APPLICATIONS

A. Analog simulations (Ref. 1)

As a check on the basic predictions of Sec. III, we performed measurements on an analog electrical circuit obeying the driven Duffing equation:

$$\ddot{x} + \gamma \dot{x} + ax + \beta x^3 = A \cos(\omega t) + \lambda , \tag{4.1}$$

$$\lambda = \lambda_0 + \delta \cos(\Omega t) . \tag{4.2}$$

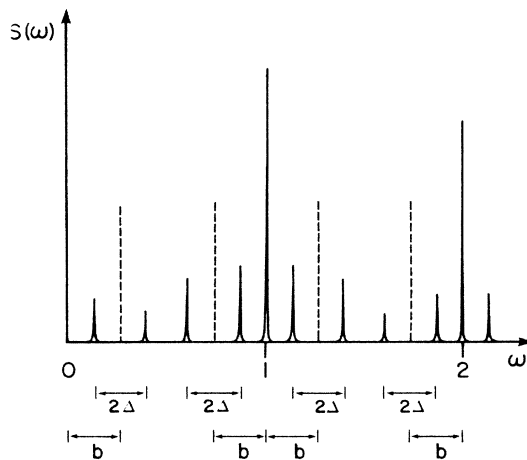


FIG. 4. Predicted power spectrum $S(\omega)$ for a periodically perturbed system near the onset of a Hopf bifurcation, as given by Eq. (3.37).

With γ , α , β , and A held constant, and $\delta=0$, the parameter λ_0 was increased until a period-doubling bifurcation occurred at $\lambda_0 = \lambda_*$. According to the calculations of Sec. III, for λ_0 slightly less than λ_* , the system should be very sensitive to modulations of λ near frequencies $\Omega = (n + \frac{1}{2})\omega$, where n is an integer. For small modulation input amplitude δ , the observed power spectrum should follow Eq. (3.28) and Fig. 3.

Figure 6 shows the output of a spectrum analyzer when the modulation frequency Ω was close to $3\omega/2$ and illustrates a number of qualitative features. The input power level is -50 dB, while the output power level at this frequency is -25 dB, yielding a gain in power by a factor of about 300. This represents a relatively modest amplitude amplification, roughly by a factor of 17. As expected, the input at the single frequency Ω gives rise to a series of pairs of lines, centered at $\omega/2$, $3\omega/2$, $5\omega/2$, etc., but no lines near integer multiples of ω . Finally, the partners within each pair of lines have nearly equal amplitude, in reasonable agreement with Eq. (3.28), which predicts exact equality.

To make a more quantitative check, we varied the modulation frequency Ω , and measured the output at Ω , generating the frequency response curves shown in Fig. 7, for three different values of $\lambda_0 < \lambda_*$ —that is, for three different values of bifurcation parameter ϵ . The normalized response, plotted on the vertical axis, is given by the square root of the power spectrum $S(\Omega)$ and is normalized to the input amplitude δ . Consequently, the vertical axis of Fig. 7 gives directly the factor by which the input signal has been amplified. The horizontal axis gives the relative frequency $\Delta = \Omega - \frac{3}{2}$, where time is rescaled so that $\omega = 1$, as in the calculations of Sec. III.

The solid lines appearing in Fig. 7 represent χ^2 fits of the data to the square root of a Lorentzian, as predicted by Eq. (3.28). As expected, the response curves sharpen and grow as the bifurcation point is approached. Quantitatively, the height-width product of these curves should be independent of ϵ : We find products of 0.154, 0.150, and 0.146 for the circles, squares, and triangles, respectively.

In summary, the analog simulations agree quite well with the calculations of Sec. III for the period-doubling bifurcation. A more complete examination is in order, of course, but the few results presented here give us confi-

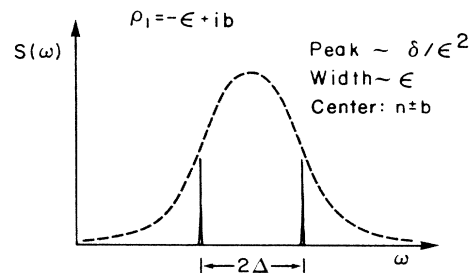


FIG. 5. Summary of the frequency response properties, valid for all four cases of Sec. III. $\text{Re}\rho_1$ governs the size and shape of the Lorentzian response curve, while $\text{Im}\rho_1$ determines the position of the pairs of spectral lines induced by the modulation.

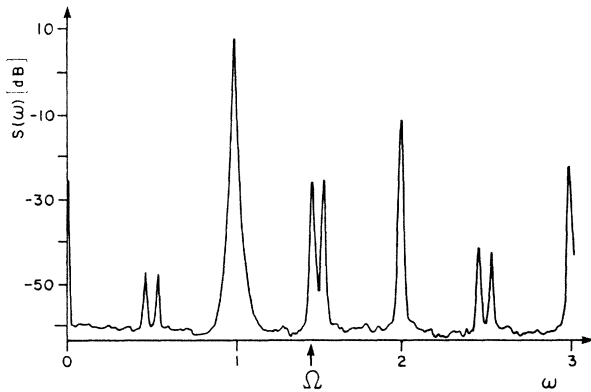


FIG. 6. Measured power spectrum of an analog simulation of the Duffing oscillator Eqs. (4.1) and (4.2), near the onset of a period-doubling bifurcation.

dence that the theoretical predictions are sensible. Along these lines, we should point out that an *independent* measurement of the bifurcation parameter ϵ would allow a more stringent test of predictions like Eq. (3.28), enabling the scaling of the height and the width—rather than the height-width product—of the response curves to be tested independently. The direct measurement of ϵ is possible—even though its value is only implicitly determined from a knowledge of the actual parameters appearing in the governing evolution equation—because it is directly related to the relaxation time of the system subject to an impulse perturbation (see Sec. II). This fact was exploited successfully to measure ϵ in experiments testing the effect of random noise on voltage-driven p - n junctions near the onset of period-doubling and Hopf bifurcations.³

B. Josephson-junction parametric amplifiers

We have seen how, near the onset of some simple instabilities, any dynamical system can act as an amplifier of small coherent modulations. The following question immediately arises: Can this notion be exploited for any practical applications? The purpose of this subsection is to suggest that there already exist examples of such amplifiers, which have been studied extensively in the physics literature:^{10–19} These devices are known as Josephson-junction parametric amplifiers (paramps).

The main thrust of the calculations of Sec. III is that a system's characteristic sensitivity to coherent modulations depends only on the type of instability encountered and is wholly independent of the physical details of the system. The original idea to use a device based on the Josephson junction as an amplifier was motivated by two features. First, the natural oscillation frequencies for Josephson junctions are in the range 10–100 GHz, where useful amplifiers have been difficult to realize. (Currently, devices known as superconductor-insulator-superconductor mixers are the best amplifiers in this frequency regime.²⁷) Second, as superconducting devices they were expected to

be low-dissipation and low-noise instruments. Curiously, it has been due to poor noise characteristics that the Josephson paramps thus far have failed to become useful devices, despite the fact that good signal gain has been achieved.^{10–13} The origin of the high-noise levels has received much attention,^{14–19} and although several suggestions have been forwarded to explain the phenomenon, it is fair to say that the problem is not yet solved. In what follows, we do not address this very interesting problem. Rather, our point is that the signal gain which has been reported for this device is intimately linked to the presence of dynamical instabilities nearby in parameter space.

We should point out that a number of different amplifier schemes have been studied which employ one or several Josephson junctions. Here, we focus on the single junction devices, which may be operated in two different modes. The first mode—given the colorful name SUPARAMP (superconducting unbiased parametric amplifier) by Feldman *et al.*¹⁰—obeys the circuit equation

$$\ddot{\phi} + \gamma \dot{\phi} + \sin\phi = A \cos(\omega t) + \delta \cos(\Omega t + \xi), \quad (4.3)$$

where ϕ is the phase difference between the macroscopic wave functions across the junction, so that $\dot{\phi}$ is proportional to the voltage across the junction.²⁸ The signal amplitude δ is small, and gain can be achieved provided the signal frequency Ω is close to the pump frequency ω . Besides the peak at ω , the output power spectrum shows a sizable component at Ω and at the “idler” frequency Ω' , given by

$$\Omega + \Omega' = 2\omega. \quad (4.4)$$

The second mode of operation includes a dc bias, so that

$$\ddot{\phi} + \gamma \dot{\phi} + \sin\phi = A \cos(\omega t) + B + \delta \cos(\Omega t + \xi). \quad (4.5)$$

Despite the obvious similarity between Eqs. (4.3) and (4.5), high gain is not achieved via condition (4.4); rather, the biased mode has achieved gain with $\Omega = \omega/2$, so that

$$\Omega + \Omega' = \omega. \quad (4.6)$$

The conditions (4.4) and (4.6) have inspired the designations of four-photon paramp and three-photon paramp, respectively.

Let us focus first on the three-photon mode. An analytic theory has been worked out by Soerensen *et al.*²⁹ Based on a direct (though approximate) analysis of Eq. (4.5), they showed that the condition for infinite gain in the limit $\Omega = \omega/2$ (i.e., zero detuning) was equivalent to the condition for the onset of subharmonic oscillations of the unmodulated ($\delta = 0$) system at half the pump frequency. That is, maximum gain coincided with the onset of a period-doubling bifurcation. Experiments with real junctions³⁰ and analog simulations¹⁹ have supported this: Indeed, the appearance of subharmonic oscillations “is a useful means of showing that the maximum gain condition has just been passed.”¹⁹

A glance at Eq. (3.28) shows that this is just what one should expect, regardless of the details of the governing equation. [This is of some significance since Eq. (4.5) is a somewhat simplified representation of the actual paramp

dynamics, neglecting, for example, the quasiparticle contribution and the presence of additional tuning circuits employed in coupling in the external signal.] Without passing to the limit $\Delta=0$ (corresponding to $\Omega=\omega/2$), it is still true that maximum gain occurs at the bifurcation point $\epsilon=0$. Taking both $\epsilon\rightarrow 0$ and $\Delta\rightarrow 0$ results in the “infinite gain” of Soerensen *et al.*

Turning next to the unbiased mode [Eq. (4.3)], we deduce from condition (4.4) that the system must operate near a saddle-node bifurcation [see Eq. (3.6) and Fig. 1] to achieve good gain. Indeed, Chiao *et al.* reported the occurrence of what they termed a “phase instability” in the dynamics of their microbridge SUPARAMP’s.¹⁴ In fact, we can deduce something else about the dynamics of the unbiased system. Note that Eq. (4.3) has the symmetry discussed in case two of Sec. III. However, Eq. (3.18a) shows that the experimentally achieved condition $\Omega\approx\omega$ ($=\frac{1}{2}$ for the time scaling used in Sec. III) will *not* result in high gain, so that the amplifier is not near the onset of a symmetry-breaking instability. Consequently, in order to reach a high-gain region of parameter space for $\Omega\approx\omega$, the system must first undergo a symmetry-breaking bifurcation as A is increased from zero. That this is so would be very easy to check experimentally—the signature of a symmetry-breaking bifurcation is the appearance of even harmonics in the output power spectrum.

Recapping, the gain achieved in the three-photon, biased mode is due to the presence of a nearby period-doubling instability, while the success of the four-photon, unbiased mode is due to the presence of a saddle-node bifurcation.

As a further conclusion, we note that the *unbiased* system governed by Eq. (4.3) could be successfully operated in the three-photon mode, where $\Omega\approx\omega/2$: After all, it is well-known that the governing equation (with $\delta=0$)—which is just the equation of motion for the driven, damped pendulum—has solutions which undergo period-doubling instabilities^{15,21} (though only after the symmetry-breaking bifurcation has occurred^{21,26}). Consequently, if the parameters are tuned so that the system is near the onset of a period doubling, the same analysis of Sec. III, case three applies just as it does for the biased-junction mode.

C. Virtual Hopf phenomenon and tunable resonances

We have seen that, in order to achieve large amplification factors, both the bifurcation parameter ϵ and the detuning frequency Δ must be small. One ramification of these conditions is that the range of input frequencies Ω that are significantly amplified may be very small. Near a period-doubling instability, for example, the system acts as a small-signal amplifier for only the sequence of narrow windows centered at $\Omega=n+\frac{1}{2}$ and of width of order ϵ . Indeed, the higher the gain is made (by reducing ϵ), the narrower these windows become (see Fig. 5).

Happily, this situation can be overcome in a large class of systems, so that *all* frequencies can be amplified. This relies on the occurrence of the virtual Hopf phenomenon:^{6,7} In essence, this phenomenon allows the *centers* of the resonance curves to be continuously tuned,

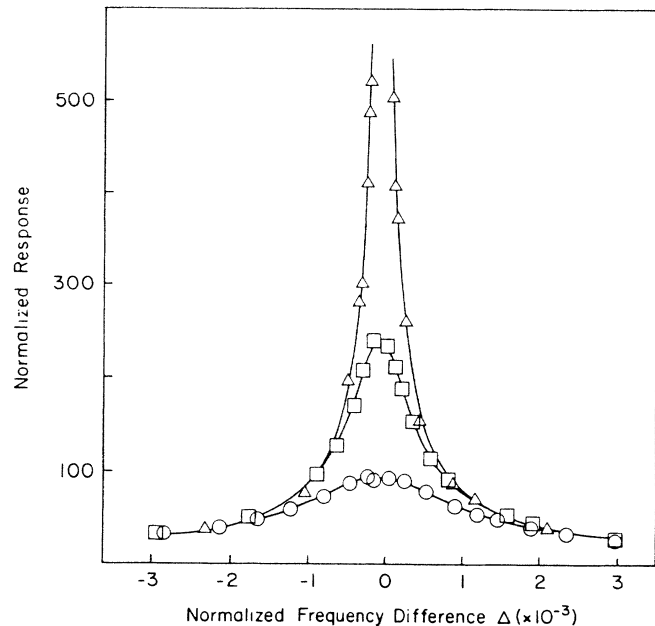


FIG. 7. Amplitude response $V(\omega)$ vs signal detuning frequency Δ , for an analog simulation of Eqs. (4.1) and (4.2). Data shown for three different parameter values, just before the onset of a period-doubling bifurcation. The circles, squares, and triangles correspond to successively smaller bifurcation parameters ϵ .

while their width remains narrow. We now give a brief review of the virtual Hopf phenomenon and then discuss its potential advantages for small-signal amplification.

The virtual Hopf is a particular kind of noisy precursor of period-doubling bifurcations, which occurs when the Floquet *multipliers* μ_k , which are related to the Floquet exponents ρ_k via the formula

$$\mu_k = e^{\rho_k T}, \quad (4.7)$$

behave as in Fig. 8. (The Floquet multipliers are simply the eigenvalues of the linearized Poincaré return map.) This behavior *must* occur, for example, between successive period-doubling bifurcations in all purely dissipative second-order nonautonomous and third-order autonomous systems, a class which includes the driven Duffing oscillator, the driven pendulum, and the Lorenz equations.⁷ From Eq. (4.7), we have (taking $T=2\pi$)

$$\ln |\mu_k| = 2\pi \operatorname{Re} \rho_k, \quad (4.8)$$

$$\arg \mu_k = 2\pi \operatorname{Im} \rho_k, \quad (4.9)$$

so that a bifurcation occurs when (at least) one of the μ_k exits the unit circle. A period doubling corresponds to $\mu_1 = -1$, while a Hopf bifurcation corresponds to a complex-conjugate pair μ_1, μ_2 with modulus unity.

To fix ideas, consider the driven pendulum equation

$$\ddot{\theta} + \gamma \dot{\theta} + \omega_0^2 \sin \theta = A \cos(\omega t). \quad (4.10)$$

Figure 8 depicts the behavior of the multipliers between successive period doublings, as the driving amplitude A is increased. This system has two Floquet multipliers, which are either both real or a complex-conjugate pair. In the latter case, the pair *must* lie on the circle

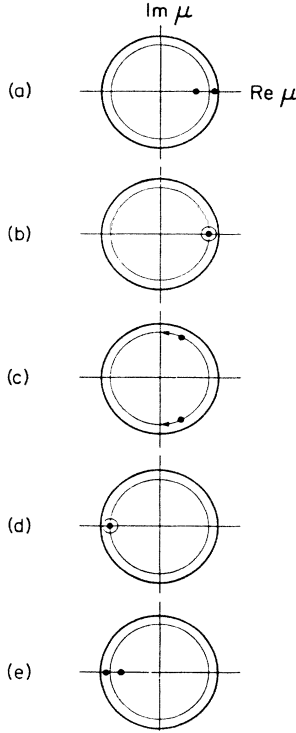


FIG. 8. Behavior of the Floquet multipliers [Eq. (4.7)] during the virtual Hopf phenomenon.

$$|\mu|^2 = e^{-\gamma T}, \quad (4.11)$$

which is a circle of constant radius lying inside the unit circle.⁷ During the sequence Figs. 8(b)–8(d), the multipliers stay the same distance from the unit circle,

$$|\mu_1| = e^{-\gamma T/2}, \quad (4.12)$$

while they slide continuously from the positive to the negative real axis,

$$0 \leq \arg \mu_1 \leq \pi. \quad (4.13)$$

From Eqs. (4.9) and (4.13), it follows that $b = \text{Im} \rho_1$ may be continuously tuned from 0 to $\frac{1}{2}$, while Eqs. (4.8) and (4.12) imply

$$\text{Re} \rho_1 = -\gamma/2 \quad (4.14)$$

so that the bifurcation parameter $\epsilon = -\text{Re} \rho_1$ remains constant. Comparison with Fig. 7 shows that the centers of the corresponding resonance curves may vary continuously over all frequencies, while the shape of the curves is fixed.

Fortuitously, this example has the additional property that *the shape and the center of the resonance curves are independently and directly tunable* during Figs. 8(b)–8(d). Ordinarily, since the values of the Floquet multipliers are only implicitly determined by the parameters appearing in the governing dynamical equation, varying any one parameter changes both the real and imaginary parts of the μ_k . But for Eq. (4.10), ϵ depends directly on γ [via Eq. (4.14)] during the virtual Hopf sequence, while A controls the continuous variation of b .

V. AUTONOMOUS SYSTEMS

We return now to the problem of small modulations of autonomous dynamical systems. We consider the same classes of codimension-1 bifurcations as in Sec. III and derive the expected power spectra $S(\omega)$. As will be shown, the form of the resulting power spectra for perturbed autonomous systems is substantially the same as the corresponding spectra for driven systems: The major differences are summarized at the end of this section.

From a computational point of view, the difference in autonomous systems is the necessary existence of the zero Floquet exponent ρ_N , so that any approximation to the full response η_m given by Eq. (2.22) must include the $k=N$ term in addition to the term(s) corresponding to the near-critical exponent(s). In fact, we can write

$$\eta_m(t) = \hat{\eta}_m(t) + \eta'_m(t), \quad (5.1)$$

where $\hat{\eta}_m$ is the contribution due to the near-critical exponents already computed in Sec. III, and η'_m is the $k=N$ term of Eq. (2.22):

$$\eta'_m(t) = \delta P_{Nm}(t) \int_0^t \left[\sum_l q_{Nl}(t') \Lambda_l(t') \right] \cos(\Omega t') dt', \quad (5.2)$$

where P_{Nm} and q_{Nl} are 2π -periodic functions of time. In all cases treated below except one—the parametrically modulated pitchfork bifurcation—the term in parentheses is 2π periodic,

$$\sum_l q_{Nl}(t') \Lambda_l(t') = \sum_n \alpha'_n e^{int'}, \quad (5.3)$$

so that Eq. (5.2) becomes

$$\eta'_m(t) = \delta P_{Nm}(t) \sum_n \alpha'_n \int_0^t e^{int'} \cos(\Omega t') dt'. \quad (5.4)$$

For the parametrically modulated pitchfork case, the $\Lambda_l(t')$ are 4π periodic and symmetric, so that

$$\sum_l q_{Nl}(t') \Lambda_l(t') = \sum_{n \text{ odd}} \tilde{\alpha}'_n e^{int'/2} \quad (5.5)$$

and Eq. (5.2) instead becomes

$$\eta'_m(t) = \delta P_{Nm}(t) \sum_{n \text{ odd}} \tilde{\alpha}'_n \int_0^t e^{int'/2} \cos(\Omega t') dt'. \quad (5.6)$$

We now proceed to the case-by-case derivations of the resulting power spectra, based on Eqs. (5.1), (5.4), and (5.6).

A. Case one: Saddle-node and transcritical bifurcations

The contribution $\hat{\eta}_m$ to the full response η_m was computed in Sec. III and is given by Eq. (3.7). From Eq. (5.4), the autonomous contribution is

$$\eta'_m = \frac{1}{2} \delta P_{Nm} \sum_n \left[\alpha'_n \frac{e^{i(n-\Omega)t} - 1}{i(n-\Omega)} + \text{c.c.} \right], \quad (5.7)$$

and under the near-resonance condition (3.6), this reduces to

$$\eta'_m = \frac{1}{2} \delta P_{Nm} \left[\frac{\alpha'_k e^{-i\Delta t}}{-i\Delta} + \text{c.c.} \right] + \delta P_{Nm} \text{Re} \left[\frac{\alpha'_k}{i\Delta} \right]. \quad (5.8)$$

Notice that the first part of this may be combined with the expression for $\hat{\eta}_m$, Eq. (3.7). Introducing the Fourier series (3.8) and

$$P_{Nm}(t) = \sum_j \beta'_j e^{ijt}, \quad (5.9)$$

the full expression for η_m becomes, from Eqs. (3.7), (5.1), and (5.8),

$$\eta_m(t) = \sum_j \left[\zeta_j e^{i(j+\Delta)t} + \text{c.c.} \right] + TP_{Nm}(t), \quad (5.10)$$

where

$$\zeta_j = \frac{1}{2} \delta \left[\frac{\beta_j \alpha_{-k}}{\epsilon + i\Delta} + \frac{\beta'_j \alpha'_{-k}}{i\Delta} \right] \quad (5.11)$$

and

$$T = \delta \text{Re} \left[\frac{\alpha'_k}{i\Delta} \right]. \quad (5.12)$$

The last term in Eq. (5.10) has the same period as the basic oscillation \mathbf{x}_0 and merely serves to renormalize the strength of the δ functions in the power spectrum at $\omega = 0, 1, 2, \dots$. We note that this effect is independent of the bifurcation parameter ϵ . Aside from these integer-frequency contributions, the power spectrum becomes

$$S_m(\omega) = \sum_j |\zeta_j|^2 [\delta(\omega - j - \Delta) + \delta(\omega - j + \Delta)]. \quad (5.13)$$

The coefficients $|\zeta_j|^2$ are *not* simply Lorentzian functions of ϵ and Δ , but are somewhat more complicated. After some algebra, one finds

$$\begin{aligned} |\zeta_j|^2 = \frac{1}{4} \delta^2 \left[\frac{|\beta_j \alpha_k|^2 + 2 \text{Re}(\beta_j \alpha_{-k} \beta'_{-j} \alpha'_k)}{\epsilon^2 + \Delta^2} \right. \\ \left. + \frac{2\epsilon}{\Delta(\Delta^2 + \epsilon^2)} \text{Im}(\beta_{-j} \alpha_k \beta'_j \alpha'_{-k}) \right. \\ \left. + \frac{|\beta'_j \alpha'_{-k}|^2}{\Delta^2} \right]. \quad (5.14) \end{aligned}$$

As a check, we do recover the nonautonomous result (3.9) by taking the primed coefficients equal to zero. Although a piece of Eq. (5.14) has the Lorentzian form, there are additional pieces having different behavior, which become particularly important for small Δ .

B. Case two: Pitchfork bifurcation

In Sec. III the symmetry considered was one in which the vector field \mathbf{F} of the unperturbed system satisfied

$$\mathbf{F}(\mathbf{x}, t) = -\mathbf{F}(-\mathbf{x}, t + T/2), \quad (5.15)$$

where T was the period of \mathbf{F} . For autonomous systems, \mathbf{F} is independent of time, so that we consider instead the situation where

$$\mathbf{F}(\mathbf{x}) = -\mathbf{F}(-\mathbf{x}). \quad (5.16)$$

Indeed, the relevance of this analysis is easily extended to the case where only some of the components of \mathbf{F} are odd

under inversion of \mathbf{x} , while others are even. For example, in the Lorentz equations^{31,32}

$$\begin{aligned} \dot{x} &= \sigma(y - x) = F_x, \\ \dot{y} &= \rho x - y - xz = F_y, \\ \dot{z} &= -\beta z + xy = F_z, \end{aligned} \quad (5.17)$$

the relevant symmetry is

$$\begin{aligned} F_x(x, y, z) &= -F_x(-x, -y, z), \\ F_y(x, y, z) &= -F_y(-x, -y, z), \\ F_z(x, y, z) &= +F_z(-x, -y, z), \end{aligned} \quad (5.18)$$

so that the modes x and y have an odd parity, while z has even parity. Consequently, if one observes the evolution of either x or y as a control parameter is varied, then a symmetry-breaking bifurcation may occur.³³

If the perturbing modulation is additive, the autonomous contribution η'_m is again given by Eq. (5.4), while $\hat{\eta}_m$ is given by Eq. (3.19a). The appropriate condition on Ω is Eq. (3.18a), which leads to

$$\eta'_m = \frac{1}{2} \delta P_{Nm} \left[\frac{\alpha'_k}{i\Delta} (1 - e^{-i\Delta t}) + \text{c.c.} \right]. \quad (5.19)$$

Introducing the Fourier series (5.9) for P_{Nm} , Eqs. (5.19) and (3.19a) combine to yield the full response

$$\begin{aligned} \eta_m = \left[\frac{1}{2} \delta \sum_j \frac{\beta'_j \alpha'_k}{i\Delta} e^{ijt} \right. \\ \left. + \frac{1}{2} \delta \sum_j \left[\frac{\beta_j \alpha_{-k}}{\epsilon + i\Delta} + \frac{\beta'_j \alpha'_{-k}}{i\Delta} \right] e^{i(j+\Delta)t} \right] + \text{c.c.} \quad (5.20) \end{aligned}$$

Recalling that our scaling of time is such that the basic *symmetric* oscillation \mathbf{x}_0 is 4π periodic, so that the unperturbed spectrum has spikes at $\omega = \frac{1}{2}, \frac{3}{2}, \frac{5}{2}, \dots$, we see that the response Eq. (5.20) *does not* contribute power to these frequencies. In this regard, the (autonomous) symmetry-breaking instability differs from the other codimension-1 bifurcations considered in this section: The presence of the zero exponent does not serve to renormalize the spikes of the unperturbed oscillation, but rather gives rise to the new lines at $\omega = 0, 1, 2, \dots$. Aside from these, the power spectrum is

$$\begin{aligned} S_m(\omega) = \frac{1}{4} \delta^2 \sum_j \left| \frac{\beta_j \alpha_{-k}}{\epsilon + i\Delta} + \frac{\beta'_j \alpha'_{-k}}{i\Delta} \right|^2 \\ \times [\delta(\omega - j - \Delta) + \delta(\omega - j + \Delta)], \quad (5.21) \end{aligned}$$

so that the strengths of the lines at $\omega = j \pm \Delta$ are no longer Lorentzian functions of ϵ and Δ , as they were for the nonautonomous case.

Turning next to parametric modulations, we have instead of Eq. (5.4) the expression (5.6) for η'_m , and the near-resonance condition is now [see Eq. (3.18b)]

$$\Omega = \frac{1}{2}k + \Delta, \quad k \text{ odd}. \quad (5.22)$$

Substitution of Eq. (5.22) into Eq. (5.6) yields *precisely* the same result, Eq. (5.19), as for the additive modulation (but with α'_k replaced by $\tilde{\alpha}'_k$). Combining this with Eq. (3.19b) for $\hat{\eta}_m$, therefore, yields the same power spectrum S_m as Eq. (5.21).

C. Case three: Period-doubling bifurcation

This time η_m is given by Eq. (3.26) and the autonomous contribution η'_m by Eq. (5.4). Upon performing the integral in Eq. (5.4), we have

$$\eta'_m = \frac{1}{2} \delta P_{Nm} \sum_n \left[\alpha'_n \frac{e^{i(n-\Omega)t} - 1}{i(n-\Omega)} + \text{c.c.} \right], \quad (5.23)$$

while the near-resonance condition on Ω is [see Eq. (3.25)]

$$\Omega = k/2 + \Delta, \quad k \text{ odd}. \quad (5.24)$$

Observe that *none* of the terms appearing in Eq. (5.23) involves a small denominator—unlike $\hat{\eta}_m$ —for the condition (5.24); consequently, the autonomous piece η'_m leads to only a minor correction to the spectrum found in the nonautonomous case. Clearly, the contribution η'_m leads to relatively weak additional lines at frequencies $\omega = n \pm \Delta$ (as well as a slight renormalization of the basic lines at $\omega = n$), the strength of these new lines being independent of the bifurcation parameter ϵ , and largely independent of the detuning Δ , as well.

We note in passing that η'_m can give a large contribution—while $\hat{\eta}_m$ becomes relatively insignificant—for a resonance condition different from Eq. (5.24), namely

$$\Omega = k + \Delta, \quad |\Delta| \ll 1. \quad (5.25)$$

Again, however, this contribution is independent of ϵ : Indeed, this resonance effect *always* exists for autonomous systems, even far from an instability, since it depends purely on the zero exponent ρ_N . This phenomenon is irrelevant to a discussion of systems' properties near the onset of bifurcations, so we pursue this point no further.

D. Case four: Hopf bifurcation

In this final case, $\hat{\eta}_m$ was computed to be that given by Eq. (3.25), while evaluation of the integral appearing in Eq. (5.4) leads to

$$\eta'_m = \frac{1}{2} \delta P_{Nm} \sum_n \left[\alpha'_n \frac{e^{i(n-\Omega)t} - 1}{i(n-\Omega)} + \text{c.c.} \right]. \quad (5.26)$$

As in Sec. III, the resonance condition is

$$\Omega = k + b + \Delta, \quad (5.27)$$

where b is the imaginary part of the near-critical Floquet exponents, so that

$$\eta'_m = \frac{1}{2} \delta P_{Nm} \left[\frac{\alpha'_k}{-i(b+\Delta)} e^{-i(b+\Delta)t} + \text{c.c.} + 2 \operatorname{Re} \left[\frac{\alpha'_k}{i(b+\Delta)} \right] \right]. \quad (5.28)$$

Combining this with Eq. (3.35) yields a total response η_m of

$$\eta_m = \frac{1}{2} \delta \sum_j \left[\frac{\beta'_j \alpha'_k}{i(b+\Delta)} e^{ijt} + \frac{\beta_j \alpha_k}{\epsilon - i\Delta} e^{i(j+b-\Delta)t} + \left[\frac{\beta'_j \alpha'_{-k}}{i(b+\Delta)} + \frac{\beta_j \alpha_{-k}}{\epsilon + i\Delta} \right] e^{i(j+b+\Delta)t} \right] + \text{c.c.}, \quad (5.29)$$

where we introduced the Fourier expansions (3.36) and (5.9) for $P_{1m}(t)$ and $P_{Nm}(t)$, respectively.

The first term in Eq. (5.29) leads to the by now familiar ϵ -independent renormalization of the integer-frequency lines in the power spectrum due to \mathbf{x}_0 . Aside from these, the power spectrum is

$$S(\omega) = \frac{1}{4} \delta^2 \sum_j \frac{|\beta_j \alpha_k|^2}{\epsilon^2 + \Delta^2} \times [\delta(\omega - j - b + \Delta) + \delta(\omega - j + b - \Delta)] + \frac{1}{4} \delta^2 \sum_j \left| \frac{\beta'_j \alpha'_{-k}}{i(b+\Delta)} + \frac{\beta_j \alpha_{-k}}{\epsilon + i\Delta} \right|^2 \times [\delta(\omega - j - b - \Delta) + \delta(\omega - j + b + \Delta)]. \quad (5.30)$$

Consequently, half of these lines have precisely the same Lorentzian dependence on ϵ and Δ as for the nonautonomous case, while the strength of the other half have a somewhat more complicated parameter dependence. However, unless b is very small—of the same order as the small parameters ϵ and Δ —the deviation of Eq. (5.30) from the nonautonomous result (3.37) is minor. Finally, one may wonder why it is that the lines at $\omega = j \pm (b + \Delta)$ have corrections due to the zero exponent, while those at $\omega = j \pm (b - \Delta)$ do not. The reason is that the modulation was chosen to be at the single frequency Ω , and this can be tuned to be near *either* $\omega = j + b$ or $\omega = j - b$; consequently, only half of the spectral lines are affected.

E. Summary

We take time out to summarize the results of this section. Comparing the calculations for autonomous systems with the corresponding cases for nonautonomous systems, we find that the extra contribution due to the zero exponent ρ_N has two effects. First, in all but the pitchfork case, the strength of the integer-frequency spikes due to the basic oscillation \mathbf{x}_0 are renormalized. This effect is independent of the bifurcation parameter ϵ , but does depend

on the detuning parameter Δ . Second, the strength of the modulation-induced lines are no longer Lorentzian functions of ϵ and Δ ; in the Hopf case this is so for only half of the lines, the other half remaining unchanged from the nonautonomous result. However, for the pitchfork and period-doubling cases, as well as the Hopf case provided the Hopf frequency b is not as small as ϵ and Δ , this deviation from a Lorentzian dependence on ϵ and Δ is relatively small, so that the nonautonomous behavior nearly matches the autonomous results.

VI. DISCUSSION

The theory developed in this paper is based on a number of approximations, so it is worthwhile to pause and reflect on how these affect the range of validity of the results. First, the bifurcation parameter ϵ is assumed small enough that a single Floquet function ϕ_k dominates the dynamical response. This enables us to find a form for the power spectrum $S(\omega)$ that depends solely on the class of the bifurcation encountered, and these classes are relatively few in number. Second, the perturbation amplitude δ is supposed small enough that the linearized Eq. (2.8) is sufficient to capture the important dynamics. For larger perturbations, one would expect the nonlinear terms to give significant corrections to the theory developed here. One interesting effect for larger δ that has been observed in period-doubling systems is to *shift* the bifurcation point of the unperturbed system.³⁴ In contrast, the linearized theory takes the basic oscillation \mathbf{x}_0 to be unchanged by the modulation, so that the onset of the dynamical instability is likewise unchanged. Recently, a theory has been developed for periodically modulated nonautonomous systems near the onset of period-doubling instabilities which explains the shifted bifurcation point, as well as predicting a number of other curious nonlinear effects.³⁴ Finally, entrainment (or frequency locking) is another effect that is beyond the scope of the theory presented here. This can occur for larger δ in modulated autonomous systems and

corresponds to a change in the frequency of the basic oscillation \mathbf{x}_0 due to the presence of the nearly resonant perturbation.

Despite the above limitations, the linearized theory seems to explain the basic features of small-signal amplification near the onset of simple bifurcations. This amplification can be quite substantial when the detuning Δ of the modulation is small. The most important feature of our analysis is that the amplification effect follows from purely dynamical considerations, regardless of the physical details of the system. Moreover, the derived results depend only on the type of bifurcation involved, which requires only the broadest, most general kind of dynamical information. For example, one may readily locate parameter values for period-doubling and Hopf instabilities in an experimental situation, even without knowledge of the governing dynamical equations.

Owing to the general dynamical nature of this amplification mechanism, one is free to choose physical realizations that provide additional advantages: The Josephson-junction paramps are attractive because they operate in an interesting frequency range and, as superconducting systems, are low-dissipation devices. Finally, as was shown in Sec. IV C, certain detailed dynamical properties might also prove desirable: The existence of the virtual Hopf phenomenon can greatly extend the frequency range over which small-signal amplification can be achieved.

ACKNOWLEDGMENTS

We thank F. Bridges, P. Bryant, J. Guckenheimer, M. Nauenberg, N. Schumaker, P. Scott, and especially D. Belanger for useful discussions. Successful design of the analog computer is due largely to the guidance of J. Crutchfield. We are indebted to J. Clarke and R. Miracky for introducing us to the subject of Josephson-junction parametric amplifiers. This work was supported by National Science Foundation Grant No. PHY-81-15541 and Division of Materials Sciences, U. S. Department of Energy, Contract No. DE-AC02-76CH00016.

*Present address: Department of Physics, Brookhaven National Laboratory, Upton, NY 11973.

¹K. Wiesenfeld and B. McNamara, *Phys. Rev. Lett.* **55**, 13 (1985).

²K. Wiesenfeld, *J. Stat. Phys.* **38**, 1071 (1985).

³C. Jeffries and K. Wiesenfeld, *Phys. Rev. A* **31**, 1077 (1985).

⁴Y. C. Chen, H. G. Winful, and J. M. Liu, *Appl. Phys. Lett.* (to be published).

⁵H. G. Winful and Y. C. Chen (unpublished).

⁶B. McNamara and K. Wiesenfeld (unpublished).

⁷K. Wiesenfeld, *Phys. Rev. A* **32**, 1744 (1985).

⁸J. P. Crutchfield, J. D. Farmer, and B. A. Huberman, *Phys. Rep.* **92**, 45 (1982).

⁹J. Heldstab, H. Thomas, T. Geisel, and B. Radons, *Z. Phys. B* **50**, 141 (1983).

¹⁰M. J. Feldman, P. T. Parrish, and R. Y. Chiao, *J. Appl. Phys.* **46**, 4031 (1975).

¹¹Y. Taur and P. L. Richards, *J. Appl. Phys.* **48**, 1321 (1977).

¹²J. Mygind, N. F. Pedersen, O. H. Soerensen, B. Duelholm, and

M. T. Levinsen, *Appl. Phys. Lett.* **35**, 91 (1979).

¹³M. T. Levinsen, N. F. Pedersen, O. H. Soerensen, B. Duelholm, and J. Mygind, *IEEE Trans. Electron Devices* **ED-27**, 1928 (1980).

¹⁴R. Y. Chiao, M. J. Feldman, D. W. Petersen, B. A. Tucker, and M. T. Levinsen, in *Future Trends in Superconductive Electronics (Charlottesville, 1978)*, Proceedings of the Conference on Future Trends in Superconductive Electronics, AIP Conf. Proc. No. 44, edited by B. S. Deaver, C. M. Falco, J. H. Harris, and S. A. Wolf (AIP, New York, 1979), p. 259.

¹⁵B. A. Huberman, J. P. Crutchfield, and N. H. Packard, *Appl. Phys. Lett.* **37**, 750 (1980).

¹⁶M. J. Feldman and M. T. Levinsen, *IEEE Trans. Magn.* **MAG-17**, 834 (1981).

¹⁷N. F. Pedersen and A. Davidson, *Appl. Phys. Lett.* **39**, 830 (1981).

¹⁸M. T. Levinsen, *J. Appl. Phys.* **53**, 4294 (1982).

¹⁹R. F. Miracky and J. Clarke, *Appl. Phys. Lett.* **43**, 508 (1983).

²⁰R. L. Kautz, *J. Appl. Phys.* **52**, 3528 (1981); **52**, 6241 (1981).

- ²¹D. D'Humieres, M. R. Beasley, B. A. Huberman, and A. Libchaber, *Phys. Rev. A* **26**, 3438 (1982).
- ²²D. W. Jordan and P. Smith, *Nonlinear Ordinary Differential Equations* (Oxford University Press, Oxford, 1977).
- ²³J. Guckenheimer and P. Holmes, *Nonlinear Oscillations, Dynamical Systems and Bifurcations of Vector Fields* (Springer, New York, 1983).
- ²⁴M. Golubitsky and D. G. Schaeffer, *Singularities and Groups in Bifurcation Theory* (Springer, New York, 1984).
- ²⁵D. H. Sattinger, *Branching in the Presence of Symmetry*, Vol. 40 of Conference Board of the Mathematical Sciences—National Science Foundation Regional Conference Series in Applied Mathematics (Society for Industrial and Applied Mathematics, Philadelphia, 1983).
- ²⁶J. W. Swift and K. Wiesenfeld, *Phys. Rev. Lett.* **52**, 705 (1984).
- ²⁷See, for example, Ref. 16.
- ²⁸B. D. Josephson, *Phys. Lett.* **1**, 251 (1962).
- ²⁹O. H. Soerensen, B. Duelholm, J. Mygind, and N. F. Pedersen, *J. Appl. Phys.* **51**, 5483 (1980).
- ³⁰N. F. Pedersen, O. H. Soerensen, B. Duelholm, and J. Mygind, *J. Low Temp. Phys.* **38**, 1 (1980).
- ³¹B. Salzmann, *J. Atmos. Sci.* **19**, 239 (1962).
- ³²E. N. Lorenz, *J. Atmos. Sci.* **20**, 130 (1963).
- ³³C. Sparrow, *The Lorenz Equations: Bifurcation, Chaos, and Strange Attractors* (Springer, New York, 1982).
- ³⁴P. Bryant and K. Wiesenfeld (unpublished).